# Precoded Faster-Than-Nyquist Signaling for Doubly Selective Underwater Acoustic Communication Channel

Jingwen Zhou, Takumi Ishihara, *Member, IEEE*, and Shinya Sugiura, *Senior Member, IEEE*

***Abstract*—In this letter, we propose faster-than-Nyquist (FTN) signaling transmission that is robust for an underwater acoustic (UWA) doubly selective channel. Owning to the explicit benefits of a reduced symbol interval specific to FTN signaling, the detrimental effects of a time-selective channel are significantly relaxed. Furthermore, upon introducing single-carrier transmit precoding and equalization, the proposed FTN signaling achieves a high detection performance. Our simulation results demonstrate that the proposed FTN signaling outperforms the conventional Nyquist-based benchmark scheme in the doubly selective channel.**

***Index Terms*—Doubly selective channel, faster-than-Nyquist signaling, underwater acoustic communication.**

## I. Introduction

UNDERWATER acoustic (UWA) communications have diverse applications, such as disaster warning, marine environment monitoring, undersea exploration, and navigation [1]. However, communications over a UWA channel are burdened with non-preferable properties, namely, a limited available bandwidth, long delay spread, and high Doppler effects [2]. For example, since the speed of sound in UWA communications is as low as $c = 1500$ m/s and the delay spread ranges tens to hundreds of milliseconds, long channel impulses are typically induced. The effects of a Doppler shift, proportional to $v/c$, is significantly higher than that of radio communications, where $v$ is the relative transmitter-receiver velocity. Time selectivity of a UWA channel is also induced by surface scattering and internal waves, where Doppler spreads are determined by wind speed and sea surface conditions [1]. Single-carrier transmission with iterative frequency-domain equalization (FDE) and orthogonal frequency-domain multiplexing (OFDM) [3] are two popular transmission techniques to solve the problems associated with a frequency-selective channel.

Furthermore, to combat the limitations imposed by a rapidly time-varying channel, several techniques have been developed for UWA communications [4]–[7]. In most previous studies, the detrimental effects of Doppler shifts are reduced by employing advanced signal processing, such as resampling and adaptive filtering. These techniques aiming to diminish the time compression/dilation induced by time-selective fading require estimation algorithms for the Doppler scaling factor. Additionally, a process is implemented to compensate for the residual Doppler effect after resampling [6], [7]. However, Doppler shift compensation based on transmit signaling has not been well explored.

The concept of faster-than-Nyquist (FTN) signaling [8], [9] has been investigated for microwave and optical communications to increase the transmission rate by reducing the symbol interval further to that defined by the time-orthogonal Nyquist criterion. An information-theoretic analysis in additive white Gaussian noise (AWGN) and frequency-flat channels shows that FTN signaling with a root-raised cosine (RRC) shaping filter achieves an information rate of the Shannon's capacity bound assuming an idealistic rectangular shaping filter, regardless of the roll-off factor of the RRC shaping filter [9]–[12]. This implies that FTN signaling is capable of exploiting the excess bandwidth that is typically wasted in the conventional Nyquist signaling with an RRC shaping filter. Moreover, FTN signaling transceivers capable of operating in a frequency-selective channel have been developed [13], [14].

Also, FTN signaling was introduced in the context of UWA communications [15]–[17] for the sake of increasing an information rate to combat the limitations imposed by the narrow available bandwidth of a UWA channel. In [15], FTN signaling channel-encoded by rateless codes as well as the low-complexity minimum mean-square error (MMSE) decision-feedback equalization (DFE) was presented for UWA communications. In [16], [17], the performance of FTN signaling with turbo equalization was investigated. Note that in [15], [16], a time-invariant UWA channel was considered. Hence, the above-mentioned previous FTN studies in UWA communications ignored the detrimental effects of a UWA-specific rapidly changing time-selective channel.

More recently, in [18], another novel benefit of FTN signaling was implied by simulation results. Specifically, FTN signaling may have the potential to have higher robustness against a time-selective channel over the conventional Nyquist signaling counterpart. This is owing to the benefits that lower symbol interval results in lower effects of a time-varying channel. However, such performance benefits of FTN signaling, especially in the context of rapidly time-varying UWA channels, have not been investigated in a quantitative manner.

Against this background, the novel contributions of this letter are as follows. Motivated by the recent FTN signaling scheme developed for time-invariant frequency-selective channel [9], [18], We present eigenvalue decomposition (EVD)-assisted FTN signaling having high robustness over a doubly

Manuscript received 25 April 2022; revised 29 June 2022; accepted 18 July 2022. Date of publication 20 July 2022; date of current version 7 October 2022. This work was supported in part by the Japan Society for the Promotion of Science (JSPS) KAKENHI under Grant 22H01481; in part by the Japan Science and Technology Agency (JST) PRESTO under Grant JPMJPR1933; and in part by JST FOREST under Grant JPMJFR2127. The associate editor coordinating the review of this article and approving it for publication was M. Kishk. *(Corresponding author: Shinya Sugiura.)*

The authors are with the Institute of Industrial Science, The University of Tokyo, Tokyo 153-8505, Japan (e-mail: sugiura@iis.u-tokyo.ac.jp).

Digital Object Identifier 10.1109/LWC.2022.3192795

selective fading channel specific to UWA communications. The proposed signaling transmitter relies on water-filling-based transmit precoding. Furthermore, the proposed FTN signaling allows us to reduce the effects of the time-varying channel upon decreasing the symbol's packing ratio $\tau$ ($\leq 1$), which represents the compression by FTN signaling. Furthermore, the proposed FTN signaling scheme dispenses with the information rate loss associated with the excess bandwidth typically imposed on the conventional Nyquist signaling with a band-limiting shaping filter. Moreover, the three-stage-concatenated turbo equalization architecture is constituted to eliminate the effects of UWA-specific doubly selective channels and those of FTN-induced inter-symbol interference.

## II. System Model

### A. Channel Model

The channel impulse response (CIR) of an *L*-tap time-varying doubly selective UWA channel is given by [3], [19]

$$c(t,\kappa) = \sum_{l=0}^{L-1} A_l(t)\delta(\kappa - \kappa_l(t)), \tag{1}$$

where $A_l(t)$ and $\kappa_l(t)$ represent the amplitude and delay of the $l$th path, respectively. For a short block length, the delay variation within a block is approximated by a first-order polynomial as follows:

$$\kappa_l(t) = \kappa_l - a_l t, \tag{2}$$

where $\kappa_l$ is the initial delay and $a_l$ is the first derivative of $\kappa_l(t)$. Hence, supposing that the amplitudes remain constant during each block, (1) can be rewritten as

$$c(t,\kappa) = \sum_{l=0}^{L-1} A_l(t)\delta(\kappa - \kappa_l + a_l t). \tag{3}$$

At the transmitter, information symbols $\mathbf{x} = [x_0,\ldots,x_{N-1}]^T \in \mathbb{C}^N$ are passed through an RRC shaping filter $h_{tr}(t)$ having a roll-off factor $\beta$ with an interval $T = \tau T_s$, where $T_s$ is the symbol interval for ISI-free transmission based on the Nyquist criterion, and $\tau \in (0,1]$ is the packing ratio for FTN transmission. Then, the signal is transmitted from a transducer, which is represented by

$$x(t) = \sum_n x_n h_{tr}(t - nT). \tag{4}$$

At the receiver, after matched filtering with $h_{re}(t) = h_{tr}^*(-t)$, the received baseband signal is represented by [20]

$$y(t) = \sum_n x_n \int_{-\infty}^{\infty} c(t,\kappa) g(t - nT - \kappa) d\kappa + z(t), \tag{5}$$

where $z(t) = \int_{-\infty}^{+\infty} n(\xi) h_{tr}^*(\xi - t)\, \mathrm{d}\,\xi$ is the associated noise, and $n(t)$ is the additive white Gaussian noise (AWGN) with zero mean and a spectral density of $N_0$. Furthermore, we have $g(t) = \int_{-\infty}^{+\infty} h_{tr}(\xi) h_{re}(t - \xi)\, \mathrm{d}\,\xi$.

Now, let us assume that the path amplitudes are constant in each block and all paths share the same Doppler scale, which is appropriate since the dominant Doppler shift comes from the relative motion between the transmitter and the receiver, and the channel coherence time is sufficiently high [21]. Then, the received samples are given by

$$y(iT) = \sum_{l=0}^{L-1} \sum_n A_l(t) x_n g((i-l-n)T) + z(iT) \tag{6}$$

$$= \sum_{l=0}^{L-1} \sum_n A_l(0) e^{j2\pi i F_d T} x_n g((i-l-n)T) + z(iT), \tag{7}$$

where $F_d$ is the maximum Doppler shift. Note that, with the aid of the resampling technique, the received samples are affected by the residual effects of the Doppler shift [7]. Also, (7) is expressed in matrix form as

$$\mathbf{y} = [y(0),\ldots,y((N-1)T)]^T \in \mathbb{C}^N \tag{8}$$

$$= \mathbf{DHx} + \mathbf{z}, \tag{9}$$

where $\mathbf{D} = \mathrm{diag}\{1, e^{j2\pi F_d T},\ldots,e^{j2\pi F_d T(N-1)}\}$ is the Doppler phase rotation matrix. The $i$th-row and $k$th-column entry of $\mathbf{H}$, which includes the effects of the RRC filter and ISI caused by the frequency-selective channel and FTN signaling, is given by $H(i,k) = \sum_{l=0}^{L-1} A_l(0) g((i-k-l)T)$.

Moreover, the covariance matrix of the noise components $\mathbf{z}$ is given by $\mathbb{E}[\mathbf{z}\mathbf{z}^H] = N_0\mathbf{G} \in \mathbb{R}^{N\times N}$, where $\mathbb{E}[\cdot]$ is the expectation operation. Note that $\mathbf{G}$ has a Toeplitz and Hermitian matrix structure and is formulated as [11]

$$\mathbf{G} = \begin{bmatrix} g_0 & g_{-1} & \cdots & g_{-(N-1)} \\ g_1 & g_0 & \cdots & g_{-(N-2)} \\ \vdots & \vdots & \ddots & \vdots \\ g_{N-1} & g_{N-2} & \cdots & g_0 \end{bmatrix}, \tag{10}$$

where $g_i = g(iT)$. Hence, we arrive at the EVD of

$$\mathbf{G} = \mathbf{Q}\mathbf{\Theta}\mathbf{Q}^T, \tag{11}$$

where $\mathbf{Q} \in \mathbb{R}^{N\times N}$ is an orthogonal matrix, and $\mathbf{\Theta} = \mathrm{diag}\{\theta_0,\ldots,\theta_{N-1}\} \in \mathbb{R}^{N\times N}$ in the descending order $\theta_0 \geq \theta_1 \geq \cdots \geq \theta_{N-1}$. Moreover, to avoid the significantly low eigenvalues intractable in the standard double-precision environment, we assume the relationship of $\tau \geq 1/(1+\beta)$, which guarantees $\theta_k > 0$ $(k = 0,\ldots,N-1)$ [18].

### B. Precoded FTN Signaling Transceiver

In the proposed scheme, we employ precoding to generate the transmitted symbols $\mathbf{x}$. More specifically, EVD-based precoding and weighting are designed for diagonalizing received blocks into parallel substreams. Assume an unprecoded information symbol block $\mathbf{s} = [s_0,\ldots,s_{N-1}]^T \in \mathbb{C}^N$ having average energy per symbol $\mathbb{E}[|s_n|^2] = \sigma_s^2$ $(n = 0,\ldots,N-1)$. The transmitted information symbol block is generated by multiplying the precoding matrix $\mathbf{P} \in \mathbb{C}^{N\times N}$ as follows:

$$\mathbf{x} = \mathbf{Ps}, \tag{12}$$

where $\mathbf{P}$ is designed under the block-based energy constraint

$$E_N = N\sigma_s^2. \tag{13}$$

The precoding matrix is optimized to maximize mutual information (MI) [18]. First, let us ignore the effects of residual phase rotations $\mathbf{D}$ since it is a challenging task to estimate $\mathbf{D}$; then, in our optimization, the received sample block is assumed to be $\mathbf{y}_h = \mathbf{H}\mathbf{x} + \mathbf{z}$ instead of (9). The approximated MI between $\mathbf{x}$ and $\mathbf{y}_h$ per block is given by

$$I(\mathbf{x};\mathbf{y}_h) = h_e(\mathbf{y}_h) - h_e(\mathbf{z}) \tag{14}$$

$$\leq \log_2((\pi e)^N \left|\mathbb{E}[\mathbf{y}_h\mathbf{y}_h^H]\right|) - \log_2\left((\pi e)^N \left|\mathbb{E}[\mathbf{z}\mathbf{z}^H]\right|\right) \tag{15}$$

$$\leq \log_2 \left|\mathbf{I}_N + \frac{1}{N_0}\mathbf{H}\mathbb{E}[\mathbf{x}\mathbf{x}^H]\mathbf{H}^H\mathbf{G}^{-1}\right|, \tag{16}$$

where $h_e(\cdot)$ and $|\cdot|$ denote differential entropy and the determinant of a matrix, respectively. $\mathbf{I}_N$ represents the $N \times N$-sized identity matrix. Additionally, from (15) to (16), the following relationship is used: $\mathbb{E}[\mathbf{y}_h\mathbf{y}_h^H] = \mathbf{H}\mathbb{E}[\mathbf{x}\mathbf{x}^H]\mathbf{H}^H + N_0\mathbf{G}$. Since $\mathbf{G}$ is positive definite, we can further modify the upper bound of the approximated MI (16) as

$$I(\mathbf{x};\mathbf{y}_h) \leq \log_2 \left|\mathbf{I}_N + \frac{1}{N_0}\mathbb{E}[\mathbf{x}\mathbf{x}^H]\mathbf{H}^H\mathbf{Q}\boldsymbol{\Theta}^{-\frac{1}{2}}\boldsymbol{\Theta}^{-\frac{1}{2}}\mathbf{Q}^T\mathbf{H}\right|$$

$$= \log_2 \left|\mathbf{I}_N + \frac{1}{N_0}\mathbb{E}[\mathbf{x}\mathbf{x}^H]\boldsymbol{\Upsilon}^H\boldsymbol{\Upsilon}\right|, \tag{17}$$

where $\boldsymbol{\Upsilon} = \boldsymbol{\Theta}^{-\frac{1}{2}}\mathbf{Q}^T\mathbf{H}$. The matrix $\boldsymbol{\Upsilon}^H\boldsymbol{\Upsilon}$ can be decomposed by EVD into $\boldsymbol{\Upsilon}^H\boldsymbol{\Upsilon} = \mathbf{B}\boldsymbol{\Omega}\mathbf{B}^H$, where $\mathbf{B} \in \mathbb{C}^{N\times N}$ is an orthogonal matrix, and $\boldsymbol{\Omega} = \mathrm{diag}\{\omega_0, \ldots, \omega_{N-1}\} \in \mathbb{R}^{N\times N}$ is a diagonal eigenvalue matrix. Hence, we arrive at

$$I(\mathbf{x};\mathbf{y}_h) \leq \log_2 \left|\mathbf{I}_N + \frac{1}{N_0}\boldsymbol{\Omega}^{\frac{1}{2}}\mathbf{B}^H\mathbb{E}[\mathbf{x}\mathbf{x}^H]\mathbf{B}\boldsymbol{\Omega}^{\frac{1}{2}}\right|. \tag{18}$$

Based on Hadamard's inequality in [18], the approximated MI of (18) is maximized when the matrix $\mathbf{B}^H\mathbb{E}[\mathbf{x}\mathbf{x}^H]\mathbf{B}$ is diagonal, i.e., $\mathbf{B}^H\mathbb{E}[\mathbf{x}\mathbf{x}^H]\mathbf{B} = \sigma_s^2\mathbf{M}$ and $\mathbf{M} = \mathrm{diag}\{\mu_0, \ldots, \mu_{N-1}\} \in \mathbb{R}^{N\times N}$. Also, if we set $\mathbf{P} = \mathbf{B}\mathbf{M}^{\frac{1}{2}}$, the approximated MI of (18) is upper-bounded as

$$I(\mathbf{x};\mathbf{y}_h) \leq \log_2 \left|\mathbf{I}_N + \frac{\sigma_s^2}{N_0}\boldsymbol{\Omega}^{\frac{1}{2}}\mathbf{M}\boldsymbol{\Omega}^{\frac{1}{2}}\right| \tag{19}$$

$$= \sum_{i=0}^{N-1} \log_2\left(1 + \frac{\sigma_s^2}{N_0}\omega_i\mu_i\right). \tag{20}$$

Note that under the assumption of perfect CSI, the approximated MI bound of (20) is maximized with respect to $\mu_i$ $(i = 0, \ldots, N-1)$. Here, the average energy per block for the precoded symbols $\mathbf{x}$ is [18]

$$E_N = \mathbb{E}\left[\mathbf{x}^H\mathbf{G}\mathbf{x}\right] \tag{21}$$

$$= \sigma_s^2 \mathrm{Tr}\left\{\mathbf{M}\mathbf{B}^H\mathbf{G}\mathbf{B}\right\} \tag{22}$$

$$= \sigma_s^2 \sum_{i=0}^{N-1} \mu_i\psi_i, \tag{23}$$

where $\mathrm{Tr}\{\cdot\}$ denotes the trace operation, and $\mathbf{B}^H\mathbf{G}\mathbf{B}$ has a diagonal elements $\psi_i$ $(i = 0, \ldots, N-1)$. From (13) and (23), the energy constraint is given by $\sigma_s^2\sum_{i=0}^{N-1}\mu_i\psi_i = N\sigma_s^2$. Therefore, the approximated MI bound of (20) is maximized under the constraint $\sum_{i=0}^{N-1}\mu_i\psi_i = N$ with the aid of the method of Lagrange multipliers. The Lagrangian function is formulated as

$$\mathcal{L} = \sum_{i=0}^{N-1} \log_2\left(1 + \frac{\sigma_s^2}{N_0}\omega_i\mu_i\right) - \lambda\left(\sum_{i=0}^{N-1}\mu_i\psi_i - N\right), \tag{24}$$

where $\lambda$ is a Lagrange multiplier. By solving $\partial\mathcal{L}/\partial\mu_i = 0$ $(\mu_i \geq 0)$, the optimal $\mu_i$ values are calculated as

$$\mu_i = \max\left(\frac{1}{\lambda\psi_i \ln 2} - \frac{N_0}{\omega_i\sigma_s^2},\ 0\right). \tag{25}$$

Note that the solution is similar to that of the singular-value decomposition (SVD)-MIMO water-filling scheme [22, Ch. 10].

At the receiver, the weighting matrix is set to $\mathbf{W} = \mathbf{B}^H\boldsymbol{\Upsilon}^H\boldsymbol{\Theta}^{-\frac{1}{2}}\mathbf{Q}^T$, making the received symbol block become

$$\mathbf{y}_w = \mathbf{W}\mathbf{y} \tag{26}$$

$$= \mathbf{W}\mathbf{D}\mathbf{H}\mathbf{x} + \mathbf{W}\mathbf{z}, \tag{27}$$

where the covariance matrix of the additive noise is calculated as $\mathbb{E}[(\mathbf{W}\mathbf{z})(\mathbf{W}\mathbf{z})^H] = \mathbf{W}\mathbb{E}[\mathbf{z}\mathbf{z}^H]\mathbf{W}^H = N_0\boldsymbol{\Omega}$, which ensures whitened noise.

For the ideal time-invariant scenario of $\mathbf{D} = \mathbf{I}_N$, (27) can be further simplified to

$$\mathbf{y}_w = \mathbf{D}\boldsymbol{\Omega}\mathbf{M}^{\frac{1}{2}}\mathbf{x} + \mathbf{W}\mathbf{z}, \tag{28}$$

where the received symbol block is diagonalized into several independent streams. Nevertheless, $\mathbf{D}$ is no longer the identity matrix in the presence of the Doppler shift, which may degrade the achievable performance. However, owing to the benefits of a reduced symbol interval $T < T_s$, in comparison to the Nyquist criterion, the effects of the Doppler shift are minimized.

Similar to [18], the detection complexity of the proposed scheme is dominated by EVD operation, which is the order of $N^3$ per block. However, the recent fast Fourier transform (FFT)-based approximation [23] allows us to reduce it to $N \log N$.

TABLE I
BASIC PARAMETERS USED IN THE SIMULATIONS

| | |
|---|---|
| Bandwidth | 5 kHz |
| Block length | $N = 200$ |
| Target rate | $R = 1$ bps/Hz |
| Nyquist symbol interval | $T_s = 2 \times 10^{-4}$ s |
| Shaping filter | RRC |
| Roll-off | $\beta = 0.25$ |
| Packing ratio | $\tau = 0.8$ |
| Channel | Doubly-selective |
| Number of paths | 7 [2] |
| Delay spread | 10.7 ms |
| Max. normalized Doppler freq. | $F_dT_s = 1.2 \times 10^{-4}$ |

## III. PERFORMANCE RESULTS

In this section, the achievable performance of the proposed scheme is evaluated in terms of bit error ratio (BER) under different scenarios, where the basic system parameters are listed in Table I. Three-stage-concatenated turbo coding is employed as a channel encoder [24]. The bit loading part is applied to

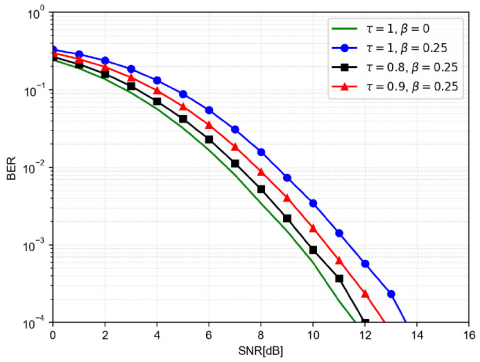


Fig. 1. BER comparisons between the proposed FTN signaling and that of the classic Nyquist criterion with a block size of $N = 200$ and a target rate of $R = 1$ bps/Hz. The normalized Doppler shift was fixed as $1.2 \times 10^{-4}$. The packing ratio of FTN signaling was given by $\tau \in \{0.8, 0.9\}$.

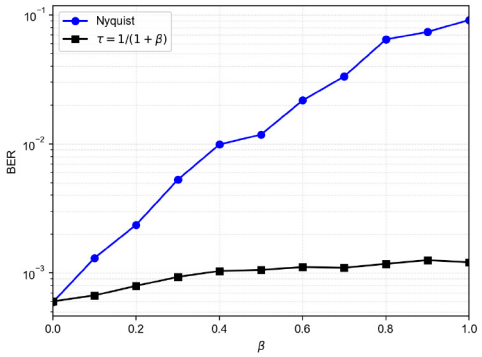


Fig. 2. Effects of roll-off factor $\beta$ on achievable BER performance of the proposed FTN signaling scheme and the Nyquist-criterion counterpart for $R = 1$ bps/Hz, $N = 200$, $\sigma_s^2/N_0 = 10\,\mathrm{dB}$, and $F_d T_s = 1.2 \times 10^{-4}$.

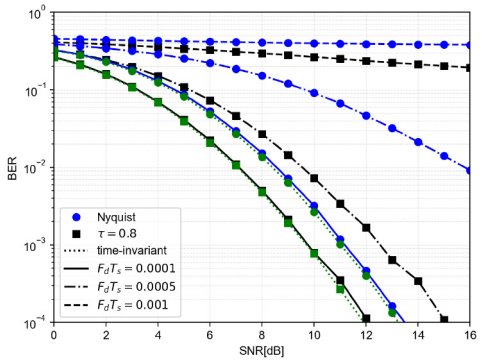


Fig. 3. BER performance of the proposed scheme and the conventional Nyquist-criterion scheme for different normalized Doppler shifts at a target rate of $R = 1$ bps/Hz. Both the schemes employed an RRC filter with $\beta = 0.25$, and the block size was set as $N = 200$.

allocate information bits to the activated substreams according to (25). More specifically, binary phase-shift keying (BPSK), quadrature phase-shift keying (QPSK), and $M$-ary quadrature amplitude modulation (MQAM) are assigned to each active substream to achieve a target rate. The detailed implementation is found in [23, Sec. IV-B].

We considered a doubly selective UWA channel, where the same amplitude and delay of each path as those in [2, Fig. 5] were used. The block size and the target information rate were $N = 200$ and $R = 1$ bps/Hz, respectively. The bandwidth was set to $2B_d(1 + \beta) = 5$ kHz, where the Nyquist interval was $T_s = 1/(2B_d)$.

In Fig. 1, we compared the BER performance of the proposed FTN signaling and that of the Nyquist criterion, both employing the same RRC filter with roll-off factor $\beta = 0.25$, which is a similar value to those employed in the many standards and in the previous FTN signaling studies [9], [16]. The normalized Doppler shift was fixed as $1.2 \times 10^{-4}$. The packing ratio of FTN signaling was given by $\tau = 0.8$ and 0.9. The curves of the Nyquist criterion employing the idealistic rectangular shaping filter ($\beta = 0$) and the same RRC shaping filter as that of the proposed scheme are also plotted as a reference, where EVD-based precoding and detection are employed in the same manner to the proposed scheme. Observe in Fig. 1 that the FTN signaling schemes outperformed the Nyquist-criterion counterpart employing the RRC shaping filter. Furthermore, the performance of FTN signaling improved upon decreasing the packing ratio from $\tau = 0.9$ to 0.8 and became closer to the ideal bound ($\tau = 1, \beta = 0$).

Fig. 2 shows the effects of roll-off factor $\beta$ on the achievable performance of the proposed FTN signaling scheme and the Nyquist-based counterpart. The SNR and the normalized Doppler frequency were given by $\sigma_s^2/N_0 = 10\,\mathrm{dB}$ and $F_d T_s = 1.2 \times 10^{-4}$, respectively. The roll-off factor was varied from $\beta = 0$ to 1 in steps of 0.1. The packing ratio of the FTN scheme was set to $\tau = 1/(1 + \beta)$ for each $\beta$. As shown in Fig. 2, the proposed FTN signaling scheme outperformed the Nyquist-criterion counterpart except for the idealistic sinc pulse scenario of $\beta = 0$. More specifically, upon increasing the $\beta$ value, the performance gain of the proposed FTN signaling scheme increased.

Fig. 3 shows BER performance of the proposed FTN signaling scheme and the Nyquist-criterion benchmark for different normalized Doppler shifts. The roll-off factor of the RRC filter and the block size were given by $\beta = 0.25$ and $N = 200$, respectively. The curves corresponding to no Doppler shift are also plotted. As seen in Fig. 3, in each $F_d T_s$ scenario, the proposed FTN signaling scheme exhibited better performance than the conventional Nyquist counterpart owing to the reduced symbol interval. This performance gain is achieved because the effective normalized Doppler shift experienced by our FTN signaling is characterized by $F_d T$, which is $\tau$ times lower than $F_d T_s$.

Fig. 4 shows the BER curves of the proposed scheme with normalized Doppler shifts of $F_d T_s = 5 \times 10^{-5}, 1 \times 10^{-4}$, and $1.2 \times 10^{-4}$ while maintaining a roll-off factor of $\beta = 0.25$. The block size was given by $N = 1000$, and the packing ratio of the proposed FTN scheme was set to $\tau = 0.8$. The Nyquist-criterion counterpart ($\tau = 1$) with $F_d T_s = 1.2 \times 10^{-4}$ is plotted for comparison. Observe in Fig. 4 that the performance of the FTN signaling scheme is affected more by $F_d T_s$ than in the $N = 200$ scenario (Fig. 3) while typically outperforming the Nyquist-criterion scheme. This is because the effects of channel rotation increase upon increasing the block size in the system model considered.

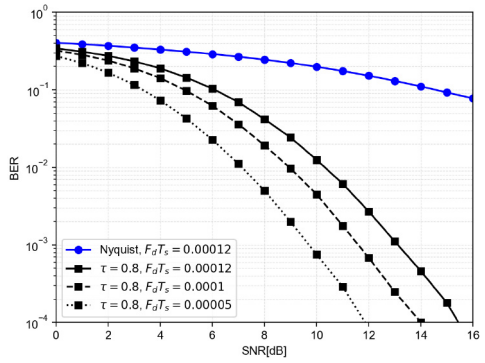


Fig. 4. BER performance of the proposed FTN scheme and the Nyquist-criterion scheme for different normalized Doppler shifts under a target rate of $R = 1$ bps/Hz. Both the schemes employed an RRC filter with $\beta = 0.25$, and we set the block size as $N = 1000$.

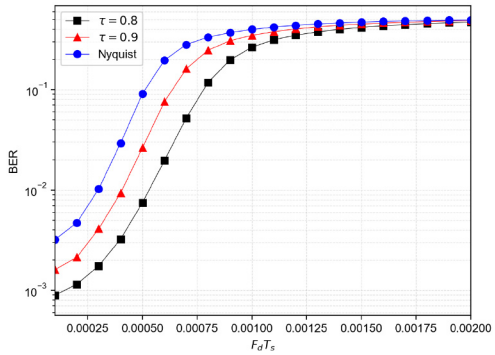


Fig. 5. Effects of normalized Doppler shift on BER performance under a target rate of $R = 1$ bps/Hz for a block size of $N = 200$ and SNR of $\sigma_s^2/N_0 = 10\,\mathrm{dB}$.

In Fig. 5, the effects of normalized Doppler shift on BER performance are illustrated with an SNR of $\sigma_s^2/N_0 = 10\,\mathrm{dB}$ and the block size fixed as $N = 200$. Both the proposed FTN signaling and the Nyquist-criterion schemes employed an RRC filter with $\beta = 0.25$. The normalized Doppler shift was varied in the range of $F_d\,T_s \in [0, 2 \times 10^{-3}]$ in steps of 0.0001. The packing ratio of the proposed scheme was given by $\tau = 0.8$ and 0.9. From Fig. 5, it can be found that the BER of both the schemes increased upon increasing $F_d\,T_s$. In the entire range of $F_d\,T_s$, the proposed FTN signaling scheme exhibited higher performance than the Nyquist-criterion benchmark.

## IV. Conclusion

In this letter, we proposed the FTN signaling scheme with EVD-based power allocation to achieve high robustness over the doubly selective UWA channel. It was demonstrated that the proposed scheme's reduced symbol interval benefits from the better BERs than the conventional Nyquist-criterion counterpart.

## References

[1] S. Al-Dharrab, M. Uysal, and T. M. Duman, "Cooperative underwater acoustic communications," *IEEE Commun. Mag.*, vol. 51, no. 7, pp. 146–153, Jul. 2013.

[2] M. Stojanovic and J. Preisig, "Underwater acoustic communication channels: Propagation models and statistical characterization," *IEEE Commun. Mag.*, vol. 47, no. 1, pp. 84–89, Jan. 2009.

[3] S. Zhou and Z. Wang, *OFDM for Underwater Acoustic Communications*. Hoboken, NJ, USA: Wiley, 2014.

[4] J. Tao, Y. R. Zheng, and C. Xiao, "Turbo detection for mobile MIMO underwater acoustic communications," in *Proc. IEEE OCEANS*, 2010, pp. 1–5.

[5] D. Wang, H. Li, Y. Xie, X. Hu, and L. Fu, "Channel-adaptive location-assisted wake-up signal detection approach based on LFM over underwater acoustic channels," *IEEE Access*, vol. 7, pp. 93806–93819, 2019.

[6] Y. Wang, J. Tao, L. Ma, M. Jiang, and W. Chen, "Joint timing and frequency synchronization for OFDM underwater acoustic communications," in *Proc. IEEE/CIC Int. Conf. Commun. China (ICCC Workshops)*, 2021, pp. 272–277.

[7] J. Han, L. Zhang, Q. Zhang, and G. Leus, "Eigendecomposition-based partial FFT demodulation for differential OFDM in underwater acoustic communications," *IEEE Trans. Veh. Technol.*, vol. 67, no. 7, pp. 6706–6710, Jul. 2018.

[8] J. Anderson, F. Rusek, and V. Öwall, "Faster-than-Nyquist signaling," *Proc. IEEE*, vol. 101, no. 8, pp. 1817–1830, Aug. 2013.

[9] T. Ishihara, S. Sugiura, and L. Hanzo, "The evolution of faster-than-Nyquist signaling," *IEEE Access*, vol. 9, pp. 86535–86564, 2021.

[10] F. Rusek and J. B. Anderson, "Constrained capacities for faster-than-Nyquist signaling," *IEEE Trans. Inf. Theory*, vol. 55, no. 2, pp. 764–775, Feb. 2009.

[11] Y. J. D. Kim, "Properties of faster-than-Nyquist channel matrices and folded-spectrum, and their applications," in *Proc. IEEE Wireless Commun. Netw. Conf.*, Apr. 2016, pp. 1–7.

[12] S. Sugiura, "Secrecy performance of Eigendecomposition-based FTN signaling and NOFDM in quasi-static fading channels," *IEEE Trans. Wireless Commun.*, vol. 20, no. 9, pp. 5872–5882, Sep. 2021.

[13] S. Sugiura and L. Hanzo, "Frequency-domain equalization aided iterative detection of faster-than-Nyquist signaling," *IEEE Trans. Veh. Technol.*, vol. 64, no. 4, pp. 2122–2128, May 2015.

[14] T. Ishihara and S. Sugiura, "Iterative frequency-domain joint channel estimation and data detection of faster-than-Nyquist signaling," *IEEE Trans. Wireless Commun.*, vol. 16, no. 9, pp. 6221–6231, Sep. 2017.

[15] U. Erez and G. Wornell, "A super-Nyquist architecture for reliable underwater acoustic communication," in *Proc. Annu. Allerton Conf. Commun. Control Comput.*, Sep. 2011, pp. 469–476.

[16] H. Qing, H. Yu, F. Ji, and D. Cao, "Turbo equalization for underwater acoustic faster-than-Nyquist signaling system," in *Proc. Int. Conf. Underwater Netw. Syst. (WUWNET)*, Atlanta, GA, USA, Oct. 2019, pp. 1–5.

[17] D. Li, Y. Wu, M. Zhu, and X. Wu, "Efficient faster-than-Nyquist transceiver design for underwater acoustic communications," in *Proc. Int. Conf. Underwater Netw. Syst. (WUWNET)*, Atlanta, GA, USA, Oct. 2019, pp. 1–5.

[18] T. Ishihara and S. Sugiura, "Eigendecomposition-precoded faster-than-Nyquist signaling with optimal power allocation in frequency-selective fading channels," *IEEE Trans. Wireless Commun.*, vol. 21, no. 3, pp. 1681–1693, Mar. 2022.

[19] W. Shi, C. He, Q. Dang, and L. Jing, "Single-carrier with index modulation for underwater acoustic communications," *Appl. Acoust.*, vol. 172, Jan. 2021, Art. no. 107572.

[20] Q. Shi, N. Wu, X. Ma, and H. Wang, "Frequency-domain joint channel estimation and decoding for faster-than-Nyquist signaling," *IEEE Trans. Commun.*, vol. 66, no. 2, pp. 781–795, Feb. 2018.

[21] B. Li, S. Zhou, M. Stojanovic, L. Freitag, and P. Willett, "Multicarrier communication over underwater acoustic channels with nonuniform doppler shifts," *IEEE J. Ocean. Eng.*, vol. 33, no. 2, pp. 198–209, Apr. 2008.

[22] A. Goldsmith, *Wireless communications*. Cambridge, U.K.: Cambridge Univ. Press, 2005.

[23] T. Ishihara and S. Sugiura, "Reduced-complexity FFT-spread multicarrier faster-than-Nyquist signaling in frequency-selective fading channel," *IEEE Open J. Commun. Soc.*, vol. 3, pp. 530–542, 2022.

[24] S. Sugiura, S. Chen, and L. Hanzo, "Coherent and differential space-time shift keying: A dispersion matrix approach," *IEEE Trans. Commun.*, vol. 58, no. 11, pp. 3219–3230, Nov. 2010.